ASMS

RESEARCH ARTICLE

Supramolecular Adducts of Cucurbit[7]uril and Amino Acids in the Gas Phase

Ekaterina Kovalenko,[1] Marta Vilaseca,[2] Mireia Díaz-Lobo,[2] A. N. Masliy,[3] Cristian Vicent,[4] Vladimir P. Fedin[1]

[1]Nikolaev Institute of Inorganic Chemistry, Siberian Branch of the Russian Academy of Sciences, Pr. Lavrentieva 3, 630090, Novosibirsk, Russia
[2]Institute for Research in Biomedicine (IRB Barcelona), The Barcelona Institute of Science and Technology, Baldiri Reixac, 10, 08028, Barcelona, Spain
[3]Kazan National Research Technological University, 420015K.Marx St 68, Kazan, Russia
[4]Serveis Centrals d'Instrumentació Científica, Universitat Jaume I, Avda. Sos Baynat s/n, E-12071, Castelló, Spain
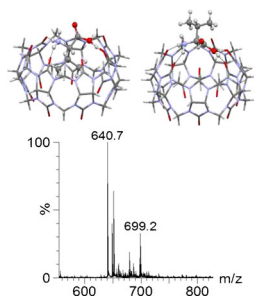
Abstract. The complexation of the macrocyclic cavitand cucurbit[7]uril (Q7) with a series of amino acids (AA) with different side chains (Asp, Asn, Gln, Ser, Ala, Val, and Ile) is investigated by ESI-MS techniques. The 1:1 $[Q7 + AA + 2H]^{2+}$ adducts are observed as the base peak when equimolar Q7:AA solutions are electrosprayed, whereas the 1:2 $[Q7 + 2AA + 2H]^{2+}$ dications are dominant when an excess of the amino acid is used. A combination of ion mobility mass spectrometry (IM-MS) and DFT calculations of the 1:1 $[Q7 + AA + 2H]^{2+}$ (AA = Tyr, Val, and Ser) adducts is also reported and proven to be unsuccessful at discriminating between exclusion or inclusion-type conformations in the gas phase. Collision induced dissociation (CID) revealed that the preferred dissociation pathways of the 1:1 $[Q7 + AA + 2H]^{2+}$ dications are strongly influenced by the identity of the amino acid side chain, whereas ion molecule reactions towards N-butylmethylamine displayed a common reactivity pattern comprising AA displacement. Special emphasis is given on the differences between the gas-phase behavior of the supramolecular adducts with amino acids (AA = Asp, Asn, Gln, Ser, Ala, Val, and Ile) and those featuring basic (Lys and Arg) and aromatic (Tyr and Phe) side chains.

Keywords: Supramolecular chemistry, Gas-phase studies, Cucurbituril, Amino acid

Introduction

The binding of amino acids to designed molecules in aqueous solution represents an important field with broad implications for basic chemical and biomedical sciences. The cucurbit[n]uril (Qn) members constitute a macrocycle family featuring a hydrophobic cavity and negatively charged portals

[1–5] suitable for amino acid, peptide, or protein binding [6, 7]. The interaction of almost the complete series of amino acids with Qn (n = 6, 7, 8) has been studied in solution by isothermal titration calorimetry (ITC) [6, 8–10], ultraviolet (UV) [11, 12], fluorescence titration (FT) [9, 13], NMR spectroscopy [14–17], and in the solid state by X-ray diffraction analysis [18, 19]. In this work, we will focus on the Q7 member of the Qn family (see Scheme 1) for which binding abilities between Q7 and amino acids or peptides in aqueous solution display characteristic 1:1 stoichiometry. The high affinity binding of Q7 with amino acids bearing an aromatic side chains relies on the enthalpic gain from ion-dipole interaction (between the positively charged amino acid and carbonyl oxygen atoms of the Qn) and the entropic gain due to the release of confined water molecules from inside the Q7 cavity [20, 21]. Additional modulation of the interaction between Q7 and amino acids

can be achieved by considering the effect of guest desolvation or the freezing of guest motion inside the cavity [10]. The complexation of Q7 with three amino acids, Phe [22], Trp [6], Tyr [10–12], a series of Phe derivatives [23] or human insulin [24] have been reported proving great potential for biological applications, including drug delivery [25–28], interactions with enzymes [29, 30], plasma membrane protein fishing [31], and label-free enzyme assays [9, 13, 32, 33].

It is instructive to extend these aqueous molecular recognition studies to the gas phase, to compare and to better understand the role of water and its effect on the hydrophobic, hydrogen-bond, or ion-dipole interactions that modulate the host–guest process. This is illustrated by the great deal of work available on amino acid complexation with cyclodextrins (CDs) hosts in the gas phase [34], making CDs interesting amino acid selectors and useful hosts in the development of analytical methods for quantifying enantiomeric excesses in the gas-phase [35]. In this sense, it becomes obvious that the most determining aspect on going from the solution to the gas phase is that in the absence of a hydrate shell, the hydrophobic effect is partly or completely lost, whereas electrostatic and polar interactions are strengthened [36, 37]. Consequently, the stability and selectivity of the supramolecular gas-phase complexes based on Q7 may not always mirror precisely its stability in the solvated state.

Gas-phase studies of the Qn family have witnessed an important advance over the past years. For example, Dearden and Kim have reported seminal works on alkali metal [38, 39], guanidinium [40], alkyldiamine [41–44], and aryldiamine [45] complexation with Qn in the gas phase [46]. Several studies that deal with the gas-phase reactivity singularities of encapsulated guest molecules such as bis-imidazolium salts [47], coordination complexes [48], small peptides [49], haloacetate anions [50], acridine orange [51], alkylammonium [52], or azoalkanes [53] in the Qn complexes have also been described. A set of mass spectrometric techniques is nowadays available to study in detail whether specific Qn-based supramolecular structures can be transferred to the gas phase. It is exemplified by the identification of threaded structures between phenylenediamine isomers and Q6 in the gas phase on the basis of its CID behavior (the threaded complex dissociated via covalent cleavages of the host and guest), distinctive ion-molecule reactivity towards alkylamines (exposure of the threaded complexes to a neutral amine produced slow addition of the amine to the complex) and ion-mobility MS [45].

Gas-phase studies of the intimate arrangement of the supramolecular adducts between Q7 and amino acids have received little attention. Recently, a comparative study of the solution and the gas-phase characteristics of supramolecular adducts between Q7 and amino acids with aromatic ($AA_{aromatic}$ Tyr, Phe, and Trp) and basic (AA_{basic} Lys, Arg, and His) side chains has been published [10]. Other examples about the interaction between amino acids and Qn in gas phase include supramolecular studies of lysine or pentalysine [54], insulin [55], or small peptides featuring lysine with Q6 and Q7 [49, 56]. However, a comprehensive gas-phase study encompassing a wide range of amino acids remains virtually unexplored. In this work, we report complexation studies between Q7 and a series of amino acids with different side chains (Asp, Asn, Gln, Ser, Ala, Val, and Ile, hereafter named AA, see Scheme 1) using a combination of ESI mass spectrometric techniques and DFT calculations. A comparative study of the gas-phase behavior under identical experimental conditions is also reported for the series of $AA_{aromatic}$ and AA_{basic} amino acids.

Experimental

The starting compounds L-alanine (Ala), L-aspartic acid (Asp), L-asparagine (Asn), L-glutamine (Gln), L-valine (Val), L-isoleucine (Ile), L-tyrosine (Tyr), L-phenylalanine (Phe), L-serine (Ser), L-Lysine·HCl (Lys), and L-arginine·HCl (Arg) of high purity grade were used as purchased. Cucurbit[7]uril (Q7; MW = 1163) ($C_{42}H_{42}N_{28}O_{14}·10H_2O$) was synthesized according to a known procedure [57]. To aqueous Q7 solutions (1 × 10^{-3} M), increasing amounts of AA (from 0.5 to 5 eqs) were added. These solutions were diluted with $H_2O:CH_3OH$ to a final concentration of 5 × 10^{-5} M and directly delivered to the ESI-MS interface of the mass spectrometer. Under these conditions, supramolecular adducts between the cavitand Q7 and amino acids were observed as proton, sodium, or potassium adducts (typically in the form $[Q7 + nAA + 2cat]^{2+}$ where n = 1, 2 and cat stands for H^+, Na^+, and K^+). Experiments carried out using $H_2O:CH_3OH$ in the presence of 1% formic acid in the final dilution step displayed identical results except that ion abundances of the proton adducts were maximized.

Electrospray Ionization Mass Spectrometry (ESI - MS), Collision Induced Dissociation (CID), and Ion-Molecule Reactions

A Q-TOF Premier mass spectrometer with an electrospray source (Waters, Manchester, UK) operating in the V-mode was used. The resolution was high enough to clearly distinguish the charge state of the identified species in all cases. The drying gas as well as the cone gas was nitrogen at a flow of 300 Lh^{-1} and 30 Lh^{-1}, respectively. The temperature of the source block was set to 100°C and the desolvation temperature was set to 150°C. A capillary voltage of 3.5 kV was used in the positive scan mode. Mass calibration was performed by using a mixture of 0.05 M NaOH and 10% formic acid (50:50) that produced a number of ions of general formula $[Na_x(HCO_2)_{x-1}]^+$ encompassing the desired m/z range for calibration purposes. Aqueous 10^{-3} M Q7 solutions and the corresponding amount of AA were mixed and diluted with $H_2O:CH_3OH$ (50:50) 1% formic acid to a final concentration of 5 × 10^{-5} M and injected for MS analysis via syringe pump directly connected to the ESI source at a flow rate of 10 μL/min. Typical sampling cone voltage was 20 V. For CID experiments, the cations of interest
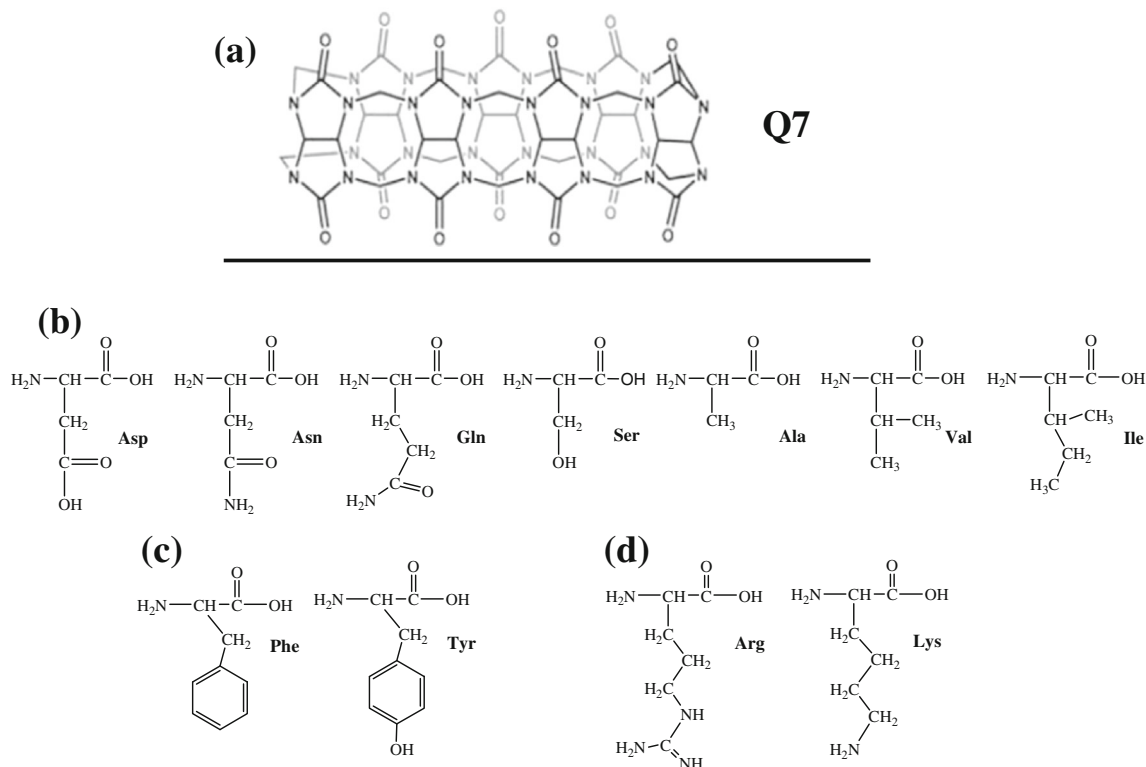
Scheme 1. (a) molecular structure of the Q7 macrocycle and the series of (b) AA (Asp, Asn, Gln, Ser, Ala, Val, Ile) amino acids; (c) AA$_{aromatic}$ (Phe and Tyr) and (d) AA$_{basic}$ (Arg and Lys)

were mass-selected using the first quadrupole (Q1) and interacted with argon in the T-wave collision cell at variable collision energies (CE$_{Elaboratory}$ = 5–40 eV) stepped by 5 eV. The ionic products of fragmentation were analyzed with the time-of-flight analyzer. The isolation width was adjusted to mass-select the complete envelope of each cation in the first quadrupole analyzer. For a qualitative analysis of the energy-dependent CID experiments, the laboratory collision energies (CE$_{Elaboratory}$) were converted to the center-of-mass frame, E_{CM} = $m/(m + M) \cdot$CE$_{Elaboratory}$, where m and M stand for the masses of the collision gas and the ionic species, respectively. For the breakdown profiles representations, signal intensities were obtained from the average of 40 scans and measuring the area of the fragmentation peaks. These graphs were represented taking into account the normalized abundance of the precursor and product ions against E_{CM}. We selected the value of the collision energy required for 50% reduction of the precursor ion ($E_{CM50\%}$) as a qualitative measure of intrinsic stability of the Q7:AA supramolecular adducts. Collision energies (CE$_{Elaboratory}$) were stepped by 2 eV near the 50% reduction of the precursor ion. Each analysis was run in triplicate and averaged to give $E_{CM50\%}$ values as listed in Figure 3. Branching ratios between the fragmentation channels were estimated from CID spectra at CE$_{Elaboratory}$ = 20 eV where secondary fragmentation pathways were not observed.

Ion-molecule reactions were conducted on a Quattro LC (quadrupole-hexapole-quadrupole) mass spectrometer with an orthogonal Z-spray-electrospray interface (Waters,

Manchester, UK). Sample solutions were infused via syringe pump directly connected to the ESI source at a flow rate of 10 μL/min, and a capillary voltage of 3.5 kV was used in the positive scan mode. The temperature of the source block was set to 100°C and the desolvation temperature was set to 150°C. The desolvation gas as well as the nebulization gas was nitrogen at a flow of 400 and 80 Lh^{-1}, respectively. The species of interest were gas-phase generated at a cone voltage of Uc = 20 V, mass-selected with Q1, and interacted with N-butylmethylamine in the hexapole collision cell, while scanning Q2 to monitor the products of ion-molecule reactions. An isolation width of ca. 2 Da was used in Q1 and the collision energy in the hexapole collision cell was nominally set to a value of CE$_{Elaboratory}$ = 0 eV to increase the residence time of the ions in the collision cell and to ensure that reactions take place at or near thermal energies. Typically, the collision gas (Argon) was passed through a U-shape tube containing 100 μL of N-butylmethylamine, so that the N-butylmethylamine substrate was introduced in the collision cell as a part of the collision gas. Ion-molecule reactions were performed using two different pressures maintained at approximately 2 × 10^{-4} mbar and 7 × 10^{-4} mbar [58, 59].

Ion Mobility Mass Spectrometry (IM-MS)

Experiments were performed on a Synapt G1 HDMS traveling wave ion mobility mass spectrometer (Waters, Manchester, UK). All samples were diluted in H$_2$O: CH$_3$OH 0.1% formic

acid at a final concentration of 2.5×10^{-6} M and placed on a 384-well plate refrigerated at 15°C. Sample introduction was made by automated chip-based nanoelectrospray using a Triversa NanoMate (Advion BioSciences, New York, USA). Ionization was performed in positive mode using a spray voltage and a gas pressure of 1.75 kV and 0.5 psi, respectively. The instrument was tuned so as to obtain a proper ion signal in the softest possible conditions to preserve solution ground state molecular structures. The source pumping speed in the backing region (5.73 mbar) of the mass spectrometer was reduced to achieve optimal transmission of noncovalent complexes. Cone voltage, extraction cone, and source temperature were set to 20 V, 5 V, and 20°C, respectively. Trap and transfer collision energies were set to 60 V. The pressure in the trap and transfer T-Wave regions were 5.93×10^{-2} mbar of Ar and the pressure in the IMS T-Wave was 0.482 mbar of N_2. Trap gas and IMS gas flows were 8 and 25 mL/s, respectively. The traveling wave used in the IMS T-Wave for mobility separation was operated at a velocity of 300 m/s. The wave amplitude was fixed to 6 V. The bias voltage for entering in the T-wave cell was 15 V. The ion mobility resolution power was 10 ($\Omega/\Delta\Omega$ full width at half maximum). This resolution power precludes the separation of potential conformers with estimated cross sections differing by less than 10% as in the case of the $[Q7 + Val + 2H]^{2+}$ and $[Q7 + Ser + 2H]^{2+}$ adducts. The instrument was mass-calibrated over the m/z range 200–2000 Da using a solution of cesium iodide. Mobility calibration was performed using tryptic peptides of known collision cross sections. The list of calibrants and calibration procedure used for traveling wave IMS experiments are given in Supplementary Figure S2. IM data were acquired and processed with MassLynx ver. 4.1 (SCN 704) and Driftscope ver. 2.4 software .

DFT Calculations

All calculations were performed within the PRIRODA program suite [60] based on Density Functional Theory ver. PBE [61]. For all the considered atoms, three valence-depleted atomic Ahlrichs basis set VTZ were used [62]. Functional PBE was shown to be effective in our earlier theoretical studies with cucurbituril [63–66]. Full gas-phase geometry optimization of all systems was carried out without any restrictions on the symmetry. Geometry optimization frequencies of normal vibrations of macromolecules were calculated. The absence of imaginary frequencies in the vibrational spectrum indicated that the optimized structures correspond to minima on the multidimensional surface of the total energy. On the basis of thermochemical analysis, the total entropy of systems were obtained, as well as total enthalpy and Gibbs free energies. In the starting structures of the Q7 and the corresponding amino acid, we located the first proton at the N-terminus, and the second one was located in different places including the carbonyl groups of the Q7, the carbonyl groups of Tyr, Val. and Ser, and the OH group from the side chain for Tyr and Ser. In all cases, the optimized structure was identical regardless the chosen starting structure. Computed cross sections were obtained from the average of the molecular areas viewed along the x, y, and z axes of the molecule [53]. We found that the computed energies for the externally-bound Q7:AA conformations are very close to those of the inclusion complexes, so that it was not possible to establish definitively which one prevails in the gas phase on the basis of only DFT calculations. As stated by Kalenius et al. [53], the energetics of the relative inclusion versus externally bound host–guest complexes is strongly dependent on the calculation methods.

Results and Discussion

Single-Stage ESI-MS of Q7:AA Mixtures

Complexation studies with the macrocyclic cavitand Q7 were carried out using a series of amino acids, hereafter labelled as AA, that features acid (Asp), amide (Asn and Gln), apolar (Ala, Val, and Ile) and polar (Ser) side chains. ESI mass spectra of equimolar Q7:Val solutions and Q7 in the presence of a 2-fold excess of Val are exemplified in Figure 1a. The 1:1 $[Q7 + AA + 2H]^{2+}$ adducts were observed as the base peak when equimolar Q7:AA solutions were electrosprayed. Prominent species of 2:2 stoichiometry formulated as $[2Q7 + 2AA + 3H]^{3+}$ were also observed. Adducts of 1:2 stoichiometry formulated as the [Q7
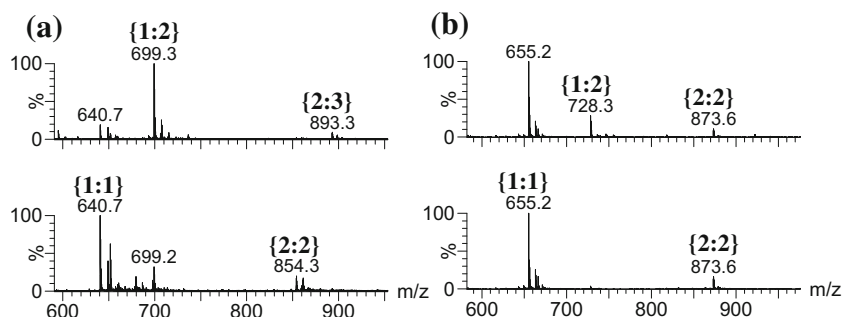

Figure 1. ESI mass spectra of Q7 and (**a**) Val and (**b**) Lys in equimolar mixtures (bottom) and using a 2-fold excess of amino acid (top) recorded under identical conditions (Uc typically 20 V). The concentration of Q7 was 5×10^{-5} M and the solvent used was $H_2O:CH_3OH$ (50:50) in the presence of 1% formic acid. Free AA is also evidenced at lower m/z values as the proton $[AA + H]^+$ adduct. The stoichiometry of the identified adducts is indicated using the {n:m} notation where n and m stands for Q7 and the amino acid stoichiometry, respectively

+ 2AA + 2H]$^{2+}$ dication were dominant when an excess of AA with respect to Q7 was used along with abundant species of 2:3 stoichiometry formulated as [2Q7 + 3AA + 3H]$^{3+}$. The 2:2 and 2:3 species were observed irrespective of the different MS conditions (desolvation temperatures or cone voltage values). In order to determine whether these adducts are due to gas-phase nonspecific or specific interactions between the Q7 and the AA, we performed identical single-stage ESI-MS experiments using more diluted sample solutions [67]. The use of sample concentrations in the 1×10^{-4} to 1×10^{-6} M range resulted invariably in the observation of 2:2 and 2:3 adducts, which suggests that these species are specific adducts likely present in the solution. Adducts of 2:3 stoichiometry are precedent in solution and they have been proposed as the dominant oligomers in milimolar aqueous solutions of Q6 and 2-methylpiperazine [68].

For the sake of comparison, we also investigated the complexation of Q7 with amino acids that bear aromatic (AA$_{aromatic}$ = Tyr and Phe) and basic (AA$_{basic}$ = Lys and Arg) side chains [10]. Whereas identical single stage ESI-MS behavior was evidenced for AA$_{aromatic}$, in terms of formation of 1:1, 1:2, 2:2, and 2:3 adducts, distinctive ESI-MS results were observed for AA$_{basic}$. In the latter case, the 1:1 [Q7 + AA$_{basic}$ + 2H]$^{2+}$ adducts were dominant irrespective of the Q7:AA$_{basic}$ ratio (see Figure 1b for Lys). Aggregates of 2:2 stoichiometry were also observed but 2:3 adducts were barely detected. These observations anticipate the unique arrangement of the supramolecular [Q7 + AA$_{basic}$ + 2H]$^{2+}$ dications in the gas phase compared with the AA and AA$_{aromatic}$ series since the doubly protonated Lys or Arg threads through the Q7 cavity [10, 54], as exemplified in Scheme 2a), thus blocking the two symmetrical portals of the Q7 and hindering the formation of complexes with 1:2 and 2:3 stoichiometry.

Contrarily, for the AA and AA$_{aromatic}$ series with a single protonation site, the protonated amino acids do not thread to the two portals of the Q7 but bind to one rim of the symmetrical Q7 macrocycle, thus leaving the second rim also available to accommodate a second protonated amino acid. This characteristic feature makes possible, besides the formation of 1:2 complexes, the formation of stable supramolecules of 2:3 stoichiometry identified by single-stage ESI-MS. Let us note that the gas-phase 1:1 [Q7 + AA + 2H]$^{2+}$ dications may adopt two dispositions as depicted in Scheme 2b for the amino acid side chain located outside of the Q7 cavity or inside of the Q7 cavity

as depicted in Scheme 2c. Supramolecular adducts depicted in Scheme 2b are known for Cys [18] and Trp [19] with Q6, whereas the arrangement depicted in Scheme 2c is precedent for Glu and tetramethylQ6 (TMeQ6) [69], on the basis of X-ray diffraction analysis.

Ion Mobility Mass Spectrometry and DFT Calculations

Further insights on the gas-phase structures of the 1:1 supramolecules of Q7 with selected amino acids (Ser, Val, and Tyr) were obtained using ion mobility mass spectrometry (IM-MS). Adduct stoichiometries, *m/z* values, experimental drift times, calibrated cross sections, and ion mobility drift time plots are given in Supplementary Table S1 and Supplementary Figure S2. Ion mobility mass spectra of the 1:1 [Q7 + AA + 2H]$^{2+}$ dications display single peaks corresponding to Ω cross sections of 212 Å^2 (Ser), 212 Å^2 (Tyr), and 216 Å^2 (Val), which are comparable to that of the [Q7 + 2Na]$^{2+}$ (cross section 212 Å^2) adduct. In the case of the 1:1 [Q7 + Tyr + 2H]$^{2+}$ adduct, this value closely resembles that reported by Kim's group (210.9 Å^2) [10]. Quantum chemical calculations were used to complement the experimental ion mobility results for the selected [Q7 + AA + 2H]$^{2+}$ (AA = Tyr, Val, and Ser) adducts and to identify the interactions that contribute to the supramolecular stabilization. Along this discussion, the most stable structures differing by less than 10 kcal·mol^{-1} were considered.

In the optimized structures of the [Q7 + Tyr + 2H]$^{2+}$ adduct, a protonation site was found at the N-terminus and the second proton was located between the carbonyl groups of the Q7 and the OH of the Tyr side chain. Both an inclusion-type structural motif (see Figure 2a) and one minimized structure in which the Tyr side chain lies outside the Q7 cavity were found. For the inclusion-type conformation, besides hydrogen-bonding interactions between the protonated N-terminal amino group with the carbonyl oxygen atoms of one Q7 rim, the aromatic ring was inserted into the cavity of Q7 while the CO$_2$H and NH$_2$ groups resided out of the cavity. Remarkably, the orientation of the buried protonated phenol group of the Tyr side chain provides further stabilization via short hydrogen bond contact with the second portal of the Q7. Such H-bonding interaction is exclusive of the Tyr amino acid and can be regarded as a threaded interaction motif; we hypothesize that it is responsible of the increased gas-phase kinetic stability of this dication as
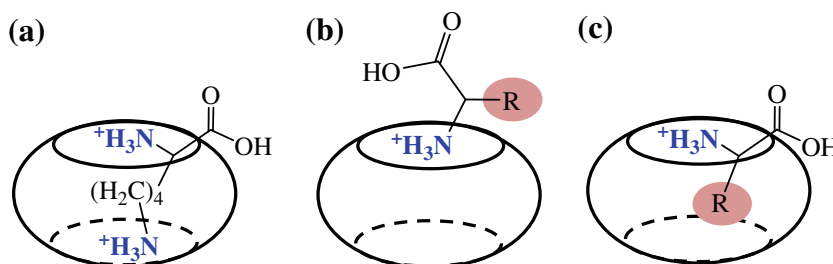
Scheme 2. Schematic drawing of (**a**) lysine threading the Q7 cavity, (**b**) and (**c**) possible amino acid side chain orientations located outside or inside of the Q7 cavity, respectively
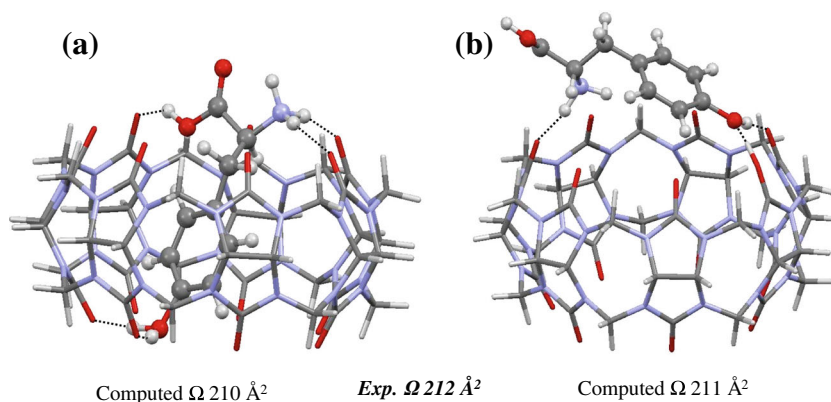
Figure 2. DFT optimized structures for the 1:1 adducts $[Q7 + Tyr + 2H]^{2+}$. Color code: O – red, N – blue, C – grey, H – white. We found an inclusion-type (**a**) and an exclusion-type (**b**) conformation. The most energetically stable form was the adduct with the protonated Tyr outside of the Q7 cavity (b-type) by 4 kcal·mol^{-1}. Computed and experimental (marked in bold and italic) cross sections are also given for both isomers

judged by its high $E_{CM(50\%)}$ value (see below). It is worth noting that the conformation for the inclusion-type arrangement optimized by the DFT calculations is similar to the crystal structure for analogous host–guest complexes with Glu. For instance, in the solid state the side chain of the Glu amino acid is hosted by the cavity of Q7, the protonated N-terminus group is more or less in the plane of the Q7 rim, and the carboxylate protrude from the Q7 rim. The exclusion-type conformation (see Figure 2b) features short H-bonding contacts between the protonated N-terminus and the phenol group with the oxygen atoms of the Q7 portals. The Tyr amino acid adopts a rather flat disposition on the plane defined by the oxygen atoms of the Q7 rim. Computed Ω values were 210 Å^2 and 211 Å^2 for the inclusion and exclusion-type conformations, respectively, which are close to the experimentally determined Ω 212 Å^2 value, thus indicating that the combined use of ion mobility and computational results was unsuccessful at discriminating between these conformations; it is also possible than multiple conformations coexist.

For Val, the minimized structures displayed the first protonation site at the N-terminus and the second proton was located

between one carbonyl group of the Q7 and the OH group of the AA establishing H-bonded interactions and stabilizing the AA:Q7 interaction. Regarding the intimate conformation of the $[Q7 + Val + 2H]^{2+}$ dication, we found one partially buried 1:1 supramolecular type (see Figure 3a) and an exclusion-type conformation (see Figure 3b) differentiated by ca. 2 kcal·mol^{-1}. According to DFT calculations, the Val side chain extends through the cavity, allowing the protonated N-terminus and the carboxylic acid to interact intimately with the Q7 rim via H-bonding. The exclusion- and inclusion-type conformations feature similar hydrogen bonding interactions between the Val and Q7, but the aliphatic side chain is located outside the cavity in the exclusion-type conformation. The experimentally determined Ω 216 Å^2 value was close to the computed Ω 215 Å^2 (exclusion-type) and 203 Å^2 (inclusion-type) cross-section values and like for Tyr, it was not possible to unambiguously discriminate between these conformations.

For Ser, the first protonation site was found at the N-terminus and the second proton was located (i) between one carbonyl group of the Q7 and the OH group of the AA (see Figure 4c) in a similar way to that found for Val, and (ii)
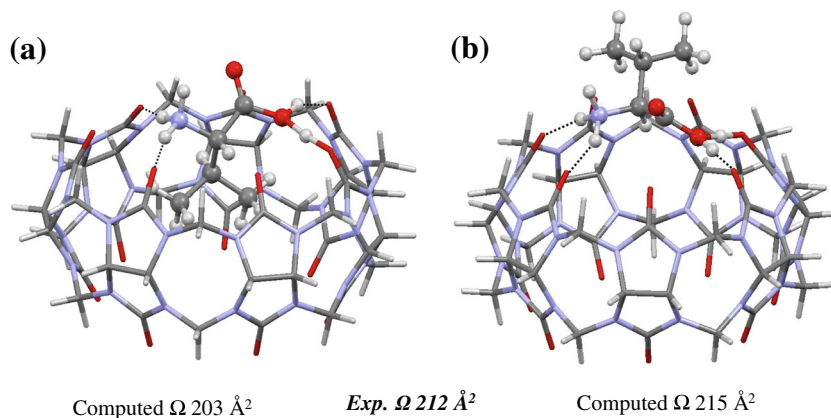

Figure 3. DFT optimized structures for the 1:1 adducts $[Q7 + Val + 2H]^{2+}$. Color code: O – red, N – blue, C – grey, H – white. We found an inclusion-type (**a**) and an exclusion-type (**b**) conformation. The adduct with the protonated Val remaining outside the Q7 cavity (b-type) was more stable by 2 kcal·mol^{-1}. Computed and experimental (marked in bold and italic) cross sections are also given for both isomers
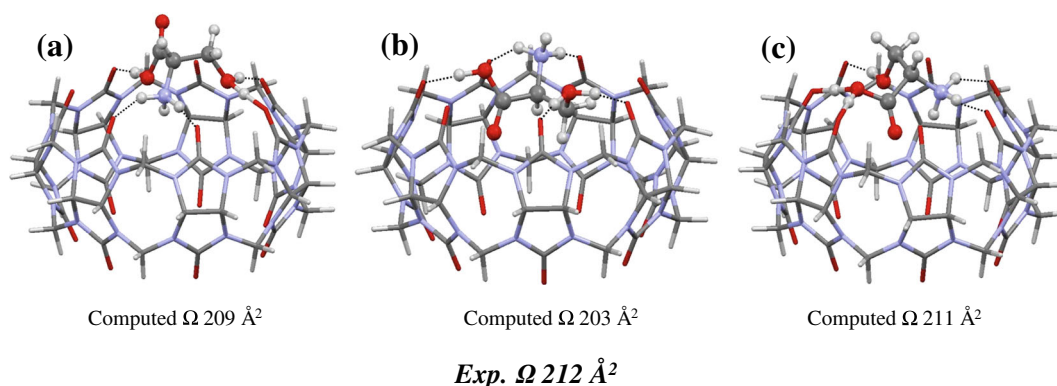
(a) Computed Ω 209 Å^2 **(b)** Computed Ω 203 Å^2 **(c)** Computed Ω 211 Å^2

Exp. Ω 212 Å^2

Figure 4. Lower energy structures for the 1:1 [Q7 + Ser + 2H]$^{2+}$ adducts. Color code: O – red, N – blue, C – grey, H – white. We found two inclusion-type (**a**) and (**b**), and an exclusion-type (**c**) conformation. The adducts with the protonated Ser remaining inside the Q7 cavity (a-type and b-type) were less stable than c-type by 10 and 2 kcal·mol^{-1}, respectively. Computed and experimental (marked in bold and italic) cross sections are also given for both isomers

between the carbonyl groups of the Q7 and the OH of the Ser side chain (see Figure 4a and b). For the [Q7 + Ser + 2H]$^{2+}$ adduct, three minimized structures were found displaying a common interaction motif that comprise short H-bonding between the protonated N-terminus and the oxygen atoms from the Q7 portal; the most stable conformation was that depicted in Figure 4c that featured the side chain externally bound with additional H-bonding between the hydroxyl groups of the C-terminus and the Ser side chain and the Q7 portals. Two additional conformations also displayed extensive H-bonding contacts between the hydroxyl groups of the C-terminus and the Ser side chain and the Q7 portals, but the Ser side chain was located partially buried in the Q7 cavity as illustrated for the conformation depicted in Figure 4b (being less stable by 2 kcal·mol^{-1}), and Figure 4a (being less stable by 10 kcal·mol^{-1}). Unlike the inclusion-type conformation found for Tyr, a threaded conformation sustained by H-bonding from the protonated N-terminus and OH with the Q7 portals is not possible for serine because of its intrinsic small size. The experimentally determined Ω 212 Å^2 value was also close to the computed Ω 211 Å^2 (exclusion-type) and 203 and 209 Å^2 (inclusion) cross-section values, which does not allow distinguishing between these conformations.

CID Mass Spectra and Ion-Molecule Reactions

We next explored the CID spectra of the 1:1 supramolecular complexes between the Q7 host and the series of AA amino

acids aimed to identify the intrinsic unimolecular reactivity patterns and to compare them with the homologs with AA$_{aromatic}$ and AA$_{basic}$ amino acids under identical experimental conditions. Characteristic CID spectra of the 1:1 adducts at increasing collision energies are presented in Supplementary Figures S3–S8. Scheme 3 shows a summary of the general fragmentation pathways observed for 1:1 complexes of Q7 with the series of AA, AA$_{aromatic}$, and AA$_{basic}$ amino acids.

CID mass spectra of the [Q7 + AA + 2H]$^{2+}$ dications displayed (i) a charge separation channel in which the protonated [Q7 + H]$^+$ and [AA + H]$^+$ cations (channel 1 in Scheme 3) were formed. A second dissociation channel that comprises amino acid evaporation was also evidenced that affords the doubly charged [Q7 + 2H]$^{2+}$ dication (channel 2 in Scheme 3). Channels 1 and 2 efficiently compete with each other, indicating that their activation barriers do not differ significantly. Similar trends in the CID spectra were observed for the [Q7 + AA$_{aromatic}$ + 2H]$^{2+}$ dications. Representative breakdown profiles for the 1:1 [Q7 + Asp + 2H]$^{2+}$, [Q7 + Gln + 2H]$^{2+}$, [Q7 + Phe + 2H]$^{2+}$, and [Q7 + Arg + 2H]$^{2+}$ adducts are shown in Supplementary Figure S9. E$_{CM(50\%)}$ values, which represent the activation energy at which half of the isolated precursor complex has decomposed, can be estimated from the breakdown profiles of the mass-selected [Q7 + AA + 2H]$^{2+}$, [Q7 + AA$_{aromatic}$ + 2H]$^{2+}$, and [Q7 + AA$_{basic}$ + 2H]$^{2+}$ (see Figure 5a). The decomposition curves reveal minor
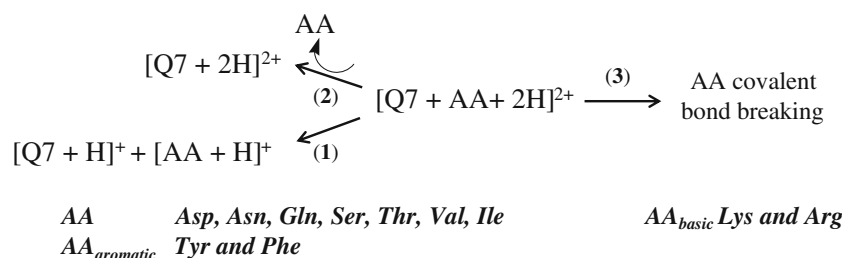
Scheme 3. General fragmentation channels observed for the 1:1 adducts of Q7 and AA, AA$_{aromatic}$ (left side) and AA$_{basic}$ (right side) upon CID conditions
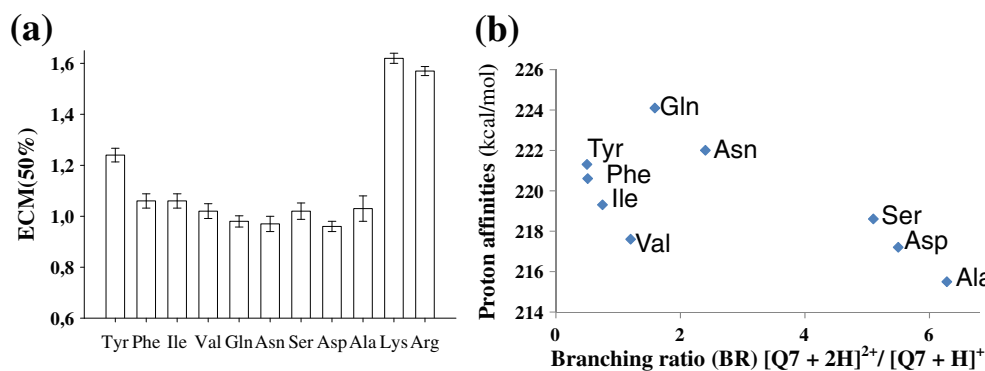
Figure 5. (**a**) $E_{CM(50\%)}$ values for the $[Q7 + AA + 2H]^{2+}$, $[Q7 + AA_{aromatic} + 2H]^{2+}$ and $[Q7 + AA_{basic} + 2H]^{2+}$ adducts, and (**b**) branching ratio (BR) for the fragmentation channel 2/1 depicted in scheme observed under CID conditions using $CE_{Elaboratory} = 20$ eV at which secondary fragmentation channels were not manifested. Standard deviations of the BR values were less than 5% from each sample run in triplicate

differences in the kinetic stability for the AA series, $E_{CM(50\%)}$ values falling within the 0.96 to 1.08 eV range. A similar $E_{CM(50\%)}$ value was determined for Phe but an enhanced $E_{CM(50\%)}$ of 1.23 eV value was observed for Tyr that can be rationalized on the basis of DFT calculations by considering the threaded conformation accompanied by an increase in the number of optimal hydrogen bonds between the phenol group and the oxygen atoms of the one of the Q7 rims (see DFT section above). We did not observe clear defined trends in the CID spectra, thus indicating that $E_{CM(50\%)}$ values were insensitive to the distinctive stabilizing effect of the amino acid side chain with the Q7 host. These observations anticipate that for the AA and AA$_{aromatic}$ series, hydrogen bonding and ion-dipole interactions between the N-terminal ammonium and the Q7 portals are the dominant stabilizing interactions, whereas a marginal effect of the side chain on the intrinsic stability of the adducts is manifested.

Conversely, the host–guest complex formed with the AA$_{basic}$ dissociated following amino acid bond cleavages while coordinated to the Q7 cavitand as dominant pathway (see channel 3 in the Scheme 3), whereas channel 1 was operative to a lesser extent. These 1:1 Q7:AA$_{basic}$ adducts are kinetically more stable than those of the remaining AA and AA$_{aromatic}$ series as evidenced by significantly higher $E_{CM(50\%)}$ values (ca. 1.6 eV). These results support that Lys and Arg, with two protonable sites, are threading through the Q7 cavitand and allow the N-terminal and basic side-chain ammonium groups to interact simultaneously with opposite carbonyl portals.

Figure 5b shows the branching ratio (BR) between the product ions associated to channel 2 and channel 1 (taken as the ion intensity ratio between the $[Q7 + 2H]^{2+}/[Q7 + H]^+$ product ions) plotted versus the proton affinities of the investigated amino acids [70]. Unlike the $E_{CM(50\%)}$ values, it was observed that the BR for the fragmentation channels 2 and 1 is highly sensitive to the the identity of the amino acid side chain. For amino acids with low gas-phase proton affinities, such as Ala and Asp, evaporation of neutral amino acid (channel 2) is

dominant, whereas for amino acids with higher proton affinities, such as Gln, Asn, Tyr, Phe, and Ile, the charge separation channel (channel 1) becomes more important. This relation can be explained by recognizing, in a very simplified way, that the two fragments, $[Q + H]^+$ and the AA, bind competitively to the bridging proton in the parent $[Q7 + AA + 2H]^{2+}$ dication. Hence, the propensity to dissociate via amino acid losses to yield $[Q7 + 2H]^{2+}$ will be higher for those amino acids with lower proton affinity as they would bind loosely to the proton at the expense of the bond of the $[Q7 + H]^+$ fragment; however, an inspection of the observed BR indicates a more complex interaction type governed by other factors. For example, Val and Ala display close proton affinities but their BR vary significantly, thus suggesting that the size of the amino acid side chain also influences the kinetic of the dissociation channels 1 and 2. A plausible explanation would be that the bulkiness of amino acid side chain may affect the directionality of the H-bonding pattern established by the protonated amino acid and the Q7 portal that ultimately affects the kinetic of the dissociation of channel 1 and 2. In addition, the inhibition of intramolecular hydrogen bonds in the guest upon Q7 complexation can also alter the intrinsic amino acid proton affinity. For example, the amino acids with the largest proton affinities, Gln and Asn, display anomalous intermediate BR values between the group of Ser, Asp, Ala and Tyr, Phe, Ile, Val amino acids. In this case, it is well-known that gas-phase proton affinities of Gln and Asn are determined by the ability of the protonated amino acid to form intramolecular hydrogen bonds in the gas-phase [71] and it is likely that the intermolecular interaction in the supramolecular 1:1 Q7:AA adduct alters intramolecular interactions in the Gln and Asn sufficiently to affect their proton affinities. This effect is reminiscent to the well-documented ability of Qn members to shift the pka of the encapsulated guests in solution [25, 74, 75]. Both the steric influence of the peripheral groups of the guest on the H-bonding directionality and the inhibition of intramolecular hydrogen bonds in the guest upon host complexation have been emphasized by Brodbelt et al. in a comprehensive study of the complexation of a wide spectrum of

amines with polyether hosts [72, 73]. Presumably, the Coulombic repulsion influences the charge separation reaction (channel 1) from the the doubly-charged $[Q7 + AA + 2H]^{2+}$ dications. Whereas channel 2 occurs in a barrier-free process to form a still doubly-protonated $[Q7 + 2H]^{2+}$ product ion, channel 1 would be operative only if a significant charge separation barrier is reached during dissociation. This separation barrier arises from Coulombic repulsion as the two charged fragments are brought together; however, its estimation is difficult to anticipate [76].

Ion-molecule reactions with N-butylmethylamine were carried out to obtain additional information about the structure of the 1:1 adducts of Q7 and the AA, $AA_{aromatic}$, and AA_{basic} series in the gas phase. Ion-molecule reactivity of supramolecular complexes between Qn and diamines proved to be diagnostic of a specific threaded molecular organization in the gas phase based on whether the guest can be displaced by a neutral amine reagent [41–45, 54]. Ion molecule reactions of the $[Q7 + AA + 2H]^{2+}$ dications (AA = Asp, Gln, Asn, Val, Ile, and Ser) and $[Q7 + AA_{aromatic} + 2H]^{2+}$ dications ($AA_{aromatic}$ = Phe and Tyr) towards N-butylmethylamine yielded the guest-exchange reaction accompanied by N-butylmethylamine uptake (see Figure 6a for the general reaction scheme and Figure 6b–d for representative spectra). At low pressures of the neutral substrate in the collision cell, the substitution ion, namely [Q7 + N-butylmethylamine + 2H]$^{2+}$ coexists with the ternary [Q7 + $2N$-butylmethylamine + 2H]$^{2+}$ product, but at higher pressures the ternary product is dominant. Ion-molecule reactions of the mass-selected $[Q7 + Lys + 2H]^{2+}$ complex towards N-butylmethylamine produced exclusive amine uptake. No trace of Lys displacement was observed (see Figure 6e) as a consequence of its intrinsic threaded arrangement or due to its higher proton affinity than N-butylmethylamine. These results indicate that the AA and $AA_{aromatic}$ amino acid guests are more loosely bound to the Q7 cavity in the gas phase than AA_{basic}, Lys.

Conclusions

The complexation of a series of amino acids AA (Asp, Asn, Gln, Ala, Val, and Ile and Ser) with the macrocyclic cavitand Q7 is presented using a panoply of ESI mass spectrometric techniques and compared with the series of $AA_{aromatic}$ (Tyr and Phe) and AA_{basic} (Lys and Arg) amino acids. The most significant difference in their intrinsic gas-phase behavior arises from the presence of a second protonable site in the amino acid side chain that can be identified from single-stage ESI-MS, CID, and ion-molecule reactions. Single-stage ESI-MS reveals similar trends for the investigated 1:1 $[Q7 + AA + 2H]^{2+}$ and the
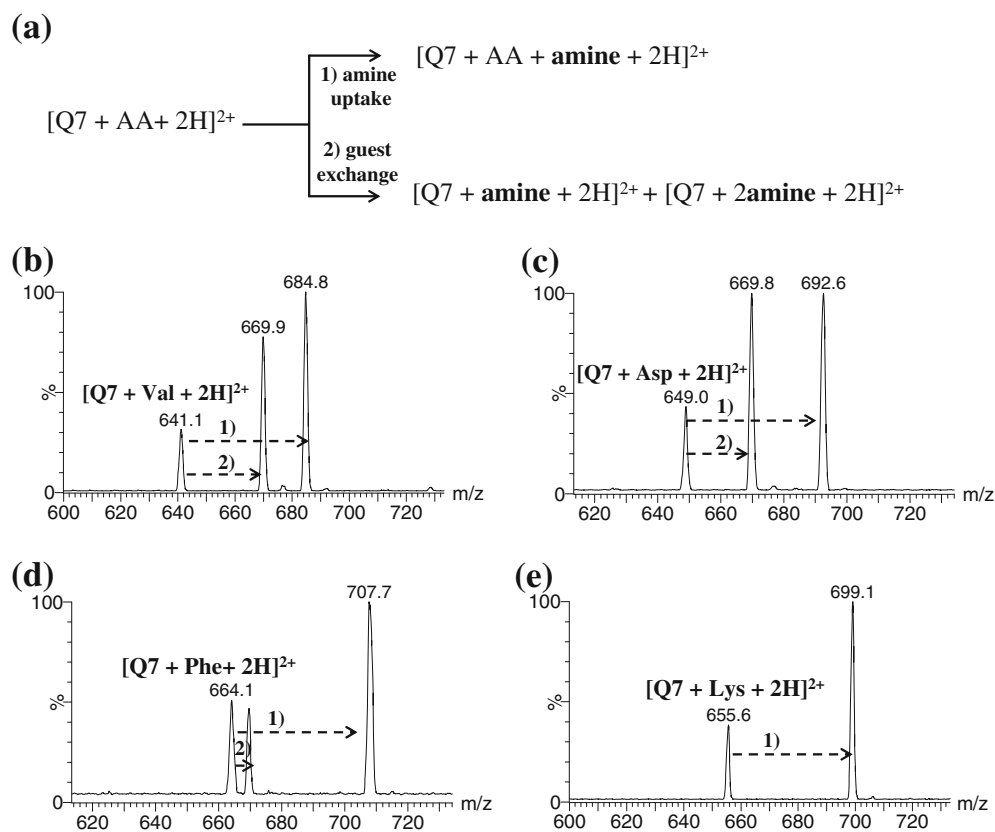

Figure 6. (a) Reactivity scheme observed for the $[Q7 + AA + 2H]^{2+}$ dications (AA = Asp, Gln, Asn, Val, Ile, and Ser) and $[Q7 + AA_{aromatic} + 2H]^{2+}$ dications with N-butylmethylamine; representative ion molecule spectra for (b) $[Q7 + Val + 2H]^{2+}$; (c) $[Q7 + Asp + 2H]^{2+}$; d) $[Q7 + Phe + 2H]^{2+}$ and e) $[Q7 + Lys + 2H]^{2+}$

1:1 $[Q7 + AA_{aromatic} + 2H]^{2+}$ adducts but different from that of the AA_{basic} series in terms of the abundance and stoichiometry of the detected adducts. The singularity of the 1:1 $[Q7 + AA_{basic} + 2H]^{2+}$ adducts is manifested in their characteristic CID spectra (essentially involving AA_{basic} bond cleavage), higher $E_{CM(50\%)}$ values than the rest of amino acids, and ion-molecule reactivity (no AA_{basic} displacement is observed). However, a similar kinetic stability is observed for the AA and $AA_{aromatic}$ series as judged by their close $E_{CM(50\%)}$ values, except for Tyr, for which an increase in the number of optimal hydrogen bonds from the phenol group together with the Q7 inclusion of the side chain allow threaded conformations to be formed that ultimately impart greater stability to the noncovalent complex. Noticeably, $E_{CM(50\%)}$ values were insensitive to the interaction effect of the amino acid side chain with the Q7 cavity or Q7 portals, and suggest that the guest fit into the Q7 cavity is not selective. This observation is reminiscent to the cyclodextrin complexes with amino acids for which gas-phase fragmentation reaction using CID, heated capillary dissociation, or blackbody infrared dissociation all proved to be insensitive to the presence of supramolecular inclusion-type complexes [77–79]. However, the expected subtle differences in the interaction modes for the supramolecular adducts of Q7 and AA and $AA_{aromatic}$ amino acids were manifested as major differences in the branching ratio for the dissociation channels via charge separating dissociation (channel 1) and amino acid evaporation (channel 2) upon CID conditions.

These experimental evidences underscore that hydrogen bonding interactions and ion-dipole attraction between the N-terminal ammonium and the Q7 portals are the dominant stabilizing interactions in the supramolecular complex in the gas phase. These observations are in sharp contrast to the known high affinity binding of the amino acids bearing aromatic side, $AA_{aromatic}$, with Q7 in aqueous solution [10, 23]. In this work, we demonstrate that despite Q7 displaying stronger binding affinities for the $AA_{aromatic}$ than the AA series in the solution, this affinity is equalized in the gas phase. It is intuitive that in the latter stages of the ESI process, the hydrated shell is stripped from the 1:1 Q7:AA adducts giving rise to a situation very different from the solution conditions. These results have implications for ESI-MS and ESI-MS/MS interpretation of closely related systems. For example, the selectivity of Q7 for the N-terminal Phe of the insulin B-chain in aqueous solution is well-documented [24]; however, it has been proven that Q7 migration from this site to other insulin B-type regions occurs in the gas phase as proven by electron capture dissociation (ECD) [55]. Our results are fully consistent with this observation from Jockusch's group [55], since on going from the solution to the gas phase the selectivity of the Q7 host for $AA_{aromatic}$ is equalized to other amino acids of the AA series so that Q7 migration to virtually any amino acid is feasible in the gas phase. Our study also illustrates that when analyzing noncovalent complexes by ESI-MS where the host–guest stabilizing energy is a combination of polar/hydrophobic interactions, the supramolecular adducts observed after the ESI process are due to the stabilizing effect of the polar interactions.

Acknowledgments

References

1. Lagona, J., Mukhopadhyay, P., Chakrabarti, S., Isaacs, L.: The cucurbit[n]uril family. Angew. Chem. Int. Ed. **44**, 4844–4870 (2005)
2. Kim, K., Selvapalam, N., Ko, Y.H., Park, K.M., Kim, D., Kim, J.: Functionalized cucurbiturils and their applications. Chem. Soc. Rev. **36**, 267–279 (2007)
3. Isaacs, L.: Cucurbit[n]urils: from mechanism to structure and function. Chem. Commun. **6**, 619–629 (2009)
4. Masson, E., Ling, X.X., Joseph, R., Kyeremeh-Mensah, L., Lu, X.Y.: Cucurbituril chemistry: a tale of supramolecular success. RSC Adv. **2**, 1213–1247 (2012)
5. Assaf, K.I., Nau, W.M.: Cucurbiturils: from synthesis to high-affinity binding and catalysis. Chem. Soc. Rev. **44**, 394–418 (2015)
6. Rajgariah, P., Urbach, A.R.: Scope of amino acid recognition by cucurbit[8]uril. J. Incl. Phenom. Macrocycl. Chem. **62**, 251–254 (2008)
7. Urbach, A.R., Ramalingam, V.: Molecular Recognition of Amino Acids, Peptides, and Proteins by Cucurbit[n] uril Receptors. Isr. J. Chem. **51**, 664–678 (2011)
8. Buschmann, H.J., Jansen, K., Schollmeyer, E.: The formation of cucurbituril complexes with amino acids and amino alcohols in aqueous formic acid studied by calorimetric titrations. Thermochim. Acta **317**, 95–98 (1998)
9. Bailey, D.M., Hennig, A., Uzunova, V.D., Nau, W.M.: Supramolecular tandem enzyme assays for multiparameter sensor arrays and enantiomeric excess determination of amino acids. Chem. Eur. J. **14**, 6069–6077 (2008)
10. Lee, J.W., Lee, H.H.L., Ko, Y.K., Kim, K., Kim, H.I.: Deciphering the specific high-affinity binding of cucurbit[7]uril to amino acids in water. J. Phys. Chem. B **119**, 4628–4636 (2015)
11. Cong, H., Tao, L.L., Yu, Y.H., Yang, F., Du, Y., Xue, S.F., Tao, Z.: Molecular recognition of aminoacid by cucurbiturils. Acta Chim. Sin. **64**, 989–996 (2006)
12. Cong, H., Tao, L.L., Yu, Y.H., Yang, F., Du, Y., Tao, Z., Xue, S.F.: Formation of host–guest complexes of amino acids and cucurbit[7] uril. Asian J. Chem. **19**, 961–964 (2007)
13. Hennig, A., Bakirci, H., Nau, W.M.: Label-free continuous enzyme assays with macrocycle-fluorescent dye complexes. Nat. Methods **4**, 629–632 (2007)
14. Liu, S.M., Ruspic, C., Mukhopadhyay, P., Chakrabarti, S., Zavalij, P.Y., Isaacs, L.: The cucurbit[n]uril family: prime components for self-sorting systems. J. Am. Chem. Soc. **127**, 15959–15967 (2005)
15. Gamal-Eldin, M.A., Macartney, D.H.: Selective molecular recognition of methylated lysines and arginines by cucurbit[6]uril and cucurbit[7]uril in aqueous solution. Org. Biomol. Chem. **11**, 488–495 (2013)
16. Kovalenko, E.A., Mainichev, D.A.: Supramolecular system of aminoacids and cucurbit[7]uril: NMR studies in solution. Appl. Magn. Reson. **46**, 281–293 (2015)
17. Kovalenko, E.A., Mainichev, D.A., Masliy, A.N., Kuznetsov, A.M.: Supramolecular chemistry of macrocyclic cavitand cucurbit[7]uril with isoleucine. Russ. Chem. Bull. **8**, 1906–1911 (2015)
18. Thuéry, P.: L-cysteine as a chiral linker in lanthanide-cucurbit[6]uril one-dimensional assemblies. Inorg. Chem. **50**, 10558–10560 (2011)

19. Danylyuk, O., Fedin, V.P.: Solid-state supramolecular assemblies of tryptophan and tryptamine with cucurbit[6]uril. Cryst. Growth Des. **12**, 550–555 (2012)

20. Biedermann, F., Uzunova, V.D., Scherman, O.A., Nau, W.M., De Simone, A.: Release of high-energy water as an essential driving force for the high-affinity binding of cucurbit[n]urils. J. Am. Chem. Soc. **134**, 15318–15323 (2012)

21. Biedermann, F., Nau, W.M., Schneider, H.-J.: The hydrophobic effect revisited—studies with supramolecular complexes imply high-energy water as a noncovalent driving force. Angew. Chem. Int. Ed. **53**, 11158–11171 (2014)

22. Jeon, W.S., Moon, K., Park, S.H., Chun, H., Ko, Y.H., Lee, J.Y., Lee, E.S., Samal, S., Selvapalam, N., Rekharsky, M.V., Sindelar, V., Sobransingh, D., Inoue, Y., Kaifer, A.E., Kim, K.: Complexation of ferrocene derivatives by the cucurbit[7]uril host: a comparative study of the cucurbituril and cyclodextrin host families. J. Am. Chem. Soc. **127**, 12984–12989 (2005)

23. Logsdon, L.A., Schardon, C.L., Ramalingam, V., Kwee, S.K., Urbach, A.R.: Nanomolar binding of peptides containing noncanonical amino acids by a synthetic receptor. J. Am. Chem. Soc. **133**, 17087–17092 (2011)

24. Chinai, J.M., Taylor, A.B., Ryno, L.M., Hargreaves, N.D., Morris, C.A., Hart, P.J., Urbach, A.R.: Molecular recognition of insulin by a synthetic receptor. J. Am. Chem. Soc. **133**, 8810–8813 (2011)

25. Saleh, N., Koner, A.L., Nau, W.M.: Activation and stabilization of drugs by supramolecular pK(a) shifts: drug-delivery applications tailored for cucurbiturils. Angew. Chem. Int. Ed. **47**, 5398–5401 (2008)

26. Kim, C., Agasti, S.S., Zhu, Z.J., Isaacs, L., Rotello, V.M.: Recognition-mediated activation of therapeutic gold nanoparticles inside living cells. Nat. Chem. **2**, 962–966 (2010)

27. Wyman, I.W., Macartney, D.H.: Host–guest complexations of local anaesthetics by cucurbit[7]uril in aqueous solution. Org. Biomol. Chem. **8**, 247–252 (2010)

28. Koner, A.L., Ghosh, I., Saleh, N., Nau, W.M.: Supramolecular encapsulation of benzimidazole-derived drugs by cucurbit[7]uril. Can. J. Chem. **89**, 139–147 (2011)

29. Hennig, A., Ghale, G., Nau, W.M.: Effects of cucurbit[7]uril on enzymatic activity. Chem. Commun. 1614–1616 (2007)

30. Ghosh, S., Isaacs, L.: Biological catalysis regulated by cucurbit[7]uril molecular containers. J. Am. Chem. Soc. **132**, 4445–4454 (2010)

31. Lee, D.W., Park, K.M., Banerjee, M., Ha, S.H., Lee, T., Suh, K., Paul, S., Jung, H., Kim, J., Selvapalam, N., Ryu, S.H., Kim, K.: Supramolecular fishing for plasma membrane proteins using an ultrastable synthetic host-guest binding pair. Nat. Chem. **3**, 154–159 (2011)

32. Nau, W.M., Ghale, G., Hennig, A., Bakirci, H., Bailey, D.M.: Substrate-selective supramolecular tandem assays: monitoring enzyme inhibition of arginase and diamine oxidase by fluorescent dye displacement from calixarene and cucurbituril macrocycles. J. Am. Chem. Soc. **131**, 11558–11570 (2009)

33. Florea, M., Nau, W.M.: Implementation of anion-receptor macrocycles in supramolecular tandem assays for enzymes involving nucleotides as substrates, products, and cofactors. Org. Biomol. Chem. **8**, 1033–1039 (2010)

34. Lebrilla, C.B.: The gas-phase chemistry of cyclodextrin inclusion complexes. Acc. Chem. Res. **34**, 653–661 (2001)

35. Grigorean, G., Ramirez, J., Ahn, S.H., Lebrilla, C.B.: A mass spectrometry method for the determination of enantiomeric excess in mixtures of d, l-amino acids. Anal. Chem. **72**, 4275–4281 (2000)

36. Bich, C., Baer, S., Jecklin, M.C., Zenobi, R.: Probing the hydrophobic effect of noncovalent complexes by mass spectrometry. J. Am. Soc. Mass Spectrom. **21**, 286–289 (2010)

37. Daniel, J.M., Friess, S.D., Rajagopalan, S., Wendt, S., Zenobi, R.: Quantitative determination of noncovalent binding interactions using soft ionization mass spectrometry. Int. J. Mass Spectrom. **216**, 1–27 (2002)

38. Mortensen, D.N., Dearden, D.V.: Influence of charge repulsion on binding strengths: experimental and computational characterization of mixed alkali metal complexes of decamethylcucurbit[5]uril in the gas phase. Chem. Commun. **47**, 6081–6083 (2011)

39. Osaka, I., Kondou, M., Selvapalam, N., Samal, S., Kim, K., Rekharsky, M.V., Inoue, Y., Arakawa, R.: Characterization of host–guest complexes of cucurbit[n]uril (n = 6, 7) by electrospray ionization mass spectrometry. J. Mass Spectrom. **41**, 202–207 (2006)

40. Yang, F., Dearden, D.V.: Guanidinium-capped cucurbit[7]uril molecular cages in the gas phase. Supramol. Chem. **23**, 53–58 (2011)

41. Zhang, H.Z., Paulsen, E.S., Walker, K.A., Krakowiak, K.E., Dearden, D.V.: Cucurbit[6]uril pseudorotaxanes: distinctive gas-phase dissociation and reactivity. J. Am. Chem. Soc. **125**, 9284–9285 (2003)

42. Zhang, H., Ferrell, T.A., Asplund, M.C., Dearden, D.V.: Molecular beads on a charged molecular string: alpha, omega-alkyldiammonium complexes of cucurbit[6]uril in the gas phase. Int. J. Mass Spectrom. **265**, 187–196 (2007)

43. Lee, S.J.C., Lee, J.W., Lee, H.H., Seo, J., Noh, D.H., Ko, Y.H., Kim, K., Kim, H.I.: Host–guest chemistry from solution to the gas phase: an essential role of direct interaction with water for high-affinity binding of cucurbit[n]urils. J. Phys. Chem. B **117**, 8855–8864 (2013)

44. Yang, F., Jones, C.A., Selvapalam, N., Ko, Y.H., Kim, K., Dearden, D.V.: Binding of alpha, omega-alkyldiammonium ions by cucurbit[n]urils in the gas phase. Supramol. Chem. **26**, 684–691 (2014)

45. Dearden, D.V., Ferrell, T.A., Asplund, M.C., Zilch, L.W., Julian, R.R., Jarrold, M.F.: One ring to bind them all: shape-selective complexation of phenylenediamine isomers with cucurbit[6]uril in the gas phase. J. Phys. Chem. A **113**, 989–997 (2009)

46. Yang, F., Dearden, D.V.: Gas phase cucurbit[n]uril chemistry. Isr. J. Chem. **51**, 551–558 (2011)

47. Cernochova, J., Branna, P., Rouchal, M., Kulhanek, P., Kuritka, I., Vicha, R.: Determination of intrinsic binding modes by mass spectrometry: gas-phase behavior of adamantylated bisimidazolium guests complexed to cucurbiturils. Chem. Eur. J. **18**, 13633–13637 (2012)

48. Mitkina, T., Fedin, V., Llusar, R., Sorribes, I., Vicent, C.: Distinctive unimolecular gas-phase reactivity of $[M(en)_2]^{2+}$ (M = Ni, Cu) dications and their inclusion complexes with the macrocyclic cavitand cucurbit[8]uril. J. Am. Soc. Mass Spectrom. **18**, 1863–1872 (2007)

49. Heo, S.W., Choi, T.S., Park, K.M., Ko, Y.H., Kim, S.B., Kim, K., Kim, H.I.: Host–guest chemistry in the gas phase: selected fragmentations of CB6-peptide complexes at lysine residues and its utility to probe the structures of small proteins. Anal. Chem. **83**, 7916–7923 (2011)

50. Choi, T.S., Ko, J.Y., Heo, S.W., Ko, Y.H., Kim, K., Kim, H.I.: Unusual complex formation and chemical reaction of haloacetate anion on the exterior surface of cucurbit[6]uril in the gas phase. J. Am. Soc. Mass Spectrom. **23**, 1786–1793 (2012)

51. Czar, M.F., Jockusch, R.A.: Understanding photophysical effects of cucurbituril encapsulation: a model study with acridine orange in the gas phase. Chem. Phys. Chem. **14**, 1138–1148 (2013)

52. Noh, D.H., Lee, S.J.C., Lee, J.W., Kim, H.I.: Host–guest chemistry in the gas phase: complex formation of cucurbit[6]uril with proton-bound water dimer. J. Am. Soc. Mass Spectrom. **25**, 410–421 (2014)

53. Lee, T.-C., Kalenius, E., Lazar, A.I., Assaf, K.I., Kuhnert, N., Grun, C.H., Janis, J., Scherman, O.A., Nau, W.M.: Chemistry inside molecular containers in the gas phase. Nat. Chem. **5**, 376–382 (2013)

54. Zhang, H., Grabenauer, M., Bowers, M.T., Dearden, D.V.: Supramolecular modification of ion chemistry: modulation of peptide charge state and dissociation behavior through complexation with cucurbit[n]uril (n = 5, 6) or alpha-cyclodextrin. J. Phys. Chem. A **113**, 1508–1517 (2009)

55. Heath, B.L., Jockusch, R.A.: Ligand migration in the gaseous insulin-CB7 complex-A cautionary tale about the use of ECD-MS for ligand binding site determination. J. Am. Soc. Mass Spectrom. **23**, 1911–1920 (2012)

56. Lee, J.W., Heo, S.W., Lee, S.J.C., Ko, J.Y., Kim, H., Kim, H.I.: Probing conformational changes of ubiquitin by host–guest chemistry using electrospray ionization mass spectrometry. J. Am. Soc. Mass Spectrom. **24**, 21–29 (2013)

57. Day, A., Arnold, A.P., Blanch, R.J., Snushall, B.: Controlling factors in the synthesis of cucurbituril and its homologues. J. Org. Chem. **66**, 8094–8100 (2001)

58. Vicent, C., Feliz, M., Llusar, R.: Intrinsic gas-phase reactivity toward methanol of trinuclear tungsten W_3S_4 complexes bearing W−X (X = Br, OH) groups. J. Phys. Chem. A **112**, 12550–12558 (2008)

59. Llusar, R., Sorribes, I., Vicent, C.: Electrospray ionization based methods for the generation of polynuclear oxo- and hydroxo group 6 anions in the gas phase. J. Clust. Sci. **20**, 177–192 (2009)

60. Laikov, D.N.: Fast evaluation of density functional exchange-correlation terms using the expansion of the electron density in auxiliary basis sets. Chem. Phys. Lett. **281**, 151–156 (1997)

61. Perdew, J.P., Burke, K., Ernzerhof, M.: Generalized gradient approximation made simple. Phys. Rev. Lett. **77**, 3865–3868 (1996)

62. Schafer, A., Horn, H., Ahlrichs, R.: Fully optimized contracted gaussin-basis sets for atoms Li to Kr. J. Chem. Phys. **97**, 2571–2577 (1992)

63. Bakovets, V.V., Masliy, A.N., Kuznetsov, A.M.: Formation thermodynamics of cucurbit[6]uril macrocycle molecules: a theory study. J. Phys. Chem. B **112**, 12010–12013 (2008)

64. Masliy, A.N., Grishaeva, T.N., Kuznetsov, A.M., Bakovets, V.V.: Quantum chemical investigation of structural and thermodynamic peculiarities of the formation of cucurbit[n]urils. J. Struct. Chem. **48**, 552–557 (2007)

65. Maslii, A.N., Grishaeva, T.N., Kuznetsov, A.M., Bakovets, V.V.: Quantum-chemical study of structurization of water in the cavity of cucurbit[6]uril. J. Struct. Chem. **50**, 391–396 (2009)

66. Grishaeva, T.N., Maslii, A.N., Kuznetsov, A.M., Bakovets, V.V.: Quantum-chemical study of the formation mechanism of cucurbit[n]uril nanocavitands. Russ. J. Inorg. Chem. **55**, 1594–1599 (2010)

67. Gabelica, V., Galic, N., De Pauw, E.: On the specificity of cyclodextrin complexes detected by electrospray mass spectrometry. J. Am. Soc. Mass Spectrom. **13**, 946–953 (2002)

68. Rekharsky, M.V., Yamamura, H., Inoue, C., Kawai, M., Osaka, I., Arakawa, R., Shiba, K., Sato, A., Ko, Y.H., Selvapalam, N., Kim, K., Inoue, Y.: Chiral recognition in cucurbituril cavities. J. Am. Chem. Soc. **128**, 14871–14880 (2006)

69. Yi, J.M., Zhang, Y.Q., Cong, H., Xue, S.F., Tao, Z.: Crystal structures of four host-guest inclusion complexes of α, α′, δ, δ′-tetramethylcucurbit[6]uril and cucurbit[8]uril with some L-amino acids. J. Mol. Struct. **933**, 112–117 (2009)

70. Hunter, E.P.L., Lias, S.G.: Evaluated gas phase basicities and proton affinities of molecules: an update. Phys. Chem. Ref. Data **27**, 413–656 (1998)

71. Bleiholde, C., Suhai, S., Paizs, B.: Revising the proton affinity scale of the naturally occurring α-amino acids. J. Am. Soc. Mass Spectrom. **17**, 1275–1281 (2006)

72. David, W.M., Brodbelt, J.S.: Threshold dissociation energies of protonated amine/polyether complexes in a quadrupole ion trap. J. Am. Soc. Mass Spectrom. **14**, 383–392 (2003)

73. Crowe, M.C., Brodbelt, J.S.: Evaluation of noncovalent interactions between peptides and polyether compounds via energy-variable collisionally activated dissociation. J. Am. Soc. Mass Spectrom. **14**, 1148–1157 (2003)

74. Ghosh, I., Nau, W.M.: The strategic use of supramolecular pK(a) shifts to enhance the bioavailability of drugs. Adv. Drug Deliv. Rev. **64**, 764–783 (2012)

75. Barooah, N., Mohanty, J., Pal, H., Bhasikuttan, A.C.: Cucurbituril-induced supramolecular pK(a) shift in fluorescent dyes and its prospective applications. Proc. Natl. Acad. Sci. India Sect. A **84**, 1–17 (2014)

76. Gronert, S.: Determining the gas-phase properties and reactivities of multiply charged ions. J. Mass Spectrom. **34**, 787–796 (1999)

77. Penn, S.G., He, F., Green, M.K., Lebrilla, C.B.: The use of heated capillary dissociation and collision-induced dissociation to determine the strength of noncovalent bonding interactions in gas-phase peptide-cyclodextrin complexes. J. Am. Soc. Mass Spectrom. **8**, 244–252 (1997)

78. Penn, S.G., He, F., Lebrilla, C.B.: Peptides complexed to cydodextrin fragment rather than dissociate when subjected to blackbody infrared radiation. J. Phys. Chem. B **102**, 9119–9126 (1998)

79. Garcia, B., Ramirez, J., Wong, S., Lebrilla, C.B.: Thermal dissociation of protonated cyclodextrin-amino acid complexes in the gas phase. Int. J. Mass Spectrom. **210/211**, 215–222 (2001)